Environmental Science Nano

ROYAL SOCIETY OF CHEMISTRY

PAPER

View Article Online
View Journal | View Issue

Cite this: *Environ. Sci.: Nano*, 2021, **8**, 502

Fluorescent plastic nanoparticles to track their interaction and fate in physiological environments†

Jessica Caldwell, [a] Roman Lehner, [a] Sandor Balog, [a] Christian Rhême, [b] Xin Gao, [b] Dedy Septiadi, [a] Christoph Weder, *[a] Alke Petri-Fink [a] and Barbara Rothen-Rutishauser *[a]

Received 10th September 2020,
Accepted 21st December 2020

DOI: 10.1039/d0en00944j

rsc.li/es-nano

As the prevalence of plastic micro- and nanoparticles in the environment, foods, and beverages continues to increase, the risk of human exposure to and uptake of such particles, notably *via* ingestion or inhalation, is also elevated. Despite this development, relatively little is known about the potential adverse effects of plastic particles on humans. The lack of relevant plastic nanoparticles for use in studies investigating their behavior and effect on human cells is a key hurdle that must be overcome prior to generating hazard data. We herein demonstrate the creation of fluorescent nanoparticles of the thermoplastic polymers poly(ethylene terephthalate), polypropylene, and polystyrene. The particles were produced by melt-processing and milling. The analysis of scanning electron microscopy images showed core diameters of less than 75 nm. Furthermore, the images revealed that the milled particles had highly heterogeneous shapes, as is often seen in environmental samples. The particles were exposed to relevant cell lines (*i.e.* Caco-2 intestinal epithelial cells and J774A.1 macrophages) to determine their uptake, assessed by confocal laser microscopy, and biocompatibility, assessed by measuring the release of lactate dehydrogenase. Exposure data showed no cytotoxicity at the concentrations utilized in this study. Interaction of the particles was found to be cell type dependent, with agglomeration on the apical surface and few intracellular particles in the intestinal epithelial cells in comparison to numerous internalized particles in the macrophages. In conclusion, the herein presented melt-processing and milling methods resulted in heterogeneously shaped plastic nanoparticles with a fluorescence label allowing their behavior within a complex biological environment to be studied.

Environmental significance

The presence of plastic micro- and nanoparticles within foods and the environment, and the subsequent exposure to and uptake of these particles by humans and animals, is a research topic that has seen an increasing level of interest to date. However, research into this topic requires the availability of nanoparticles composed of environmentally relevant plastic types. This work aims to establish a production and characterization protocol for fluorescent plastic nanoparticles of poly(ethylene terephthalate) (PET), polypropylene (PP), and polystyrene (PS) that can be tracked in biological environments.

1. Introduction

Synthetic polymers are human-made materials that display attractive, readily tunable properties that make them indispensable in our daily lives. They are used in the form of plastics, fibers, rubber, paints, and many other products. The production of plastics (the subset of polymers that is melt-processible) has skyrocketed since their introduction, with a worldwide production of 359 million tons in 2018.[1] In parallel with the production volume, the amount of plastic waste being discarded and of plastics that enter the environment through other mechanisms, notably wear, is rising continuously. While many countries have turned to disposing of this waste *via* recycling and energy recovery methods, recent estimates for the worldwide management of plastic waste indicate that 79% of all plastic waste ends up in landfills or enters the environment through other pathways.[2,3] In 2010, researchers presented numbers in the range of 4.8–12.7

[a] *Adolphe Merkle Institute, Université de Fribourg, Chemin des Verdiers 4, 1700 Fribourg, Switzerland. E-mail: christoph.weder@unifr.ch, barbara.rothen@unifr.ch*
[b] *Frewitt fabrique de machines SA, Route du Coteau 7, 1763 Granges-Paccot, Switzerland*

† Electronic supplementary information (ESI) available: Tables containing melt processing, milling, cell culturing, and DSC experimental setups. Section providing information on cryo-milled plastic microparticles, including additional descriptive figures and tables. Section providing figures and tables with additional SEM, light scattering, ζ-potential, and QCM data for ball milled plastic nanoparticles. See DOI: 10.1039/d0en00944j

million tons of mismanaged plastic waste that was discarded into the oceans alone.[4] Estimates for plastic pollution in terrestrial environments report values that are 4–23 times higher.[5]

Macroscopic plastic products (>20 cm) entering the environment have been shown to undergo degradation as a result of their exposure to ultraviolet (UV) light, chemicals, and mechanical forces exerted by wind or waves.[5] Such degradation processes lead to the formation of smaller plastic particles with dimensions at the meso (20 cm–5 mm), micro (5 mm–1 μm), and nano (<1 μm) scale.[5,6] Plastic microparticles were reported to be present in environmental samples ranging from remote arctic waters, to atmospheric fallout in urban and mountain regions, and to shorelines across the globe.[7–10] More recently, the presence of poly(ethylene terephthalate) (PET), poly(vinyl chloride) (PVC), and polystyrene (PS) plastic nanoparticles in the North Atlantic Gyre was observed.[11]

Organisms such as fish and bivalve mollusks inhabiting polluted marine environments are known to ingest plastic particles once they are present in their habitats.[12–17] Many of the aquatic organisms that have been shown to consume plastic particles are common food sources for humans. A study conducted on bivalves purchased from a fish market in China found that as many as 4.3–57.2 plastic microparticles were present in an individual bivalve.[18] However, the trophic transfer of particles from aquatic organisms to humans is not the only possible exposure pathway. Common beverages, such as bottled water and tea, have also been shown to contain plastic micro- and nanoparticles.[19,20] As a result of these contaminated foods and beverages, the average annual consumption of plastic microparticles for a single person is estimated to be 39 000–520 000 particles each year.[21] Currently no estimates exist for the ingestion of nanoparticles.

Despite the increasing possibility that plastic micro- and nanoparticles will be ingested by humans, to date relatively little work has been carried out to assess their impact on human health, in part because it is difficult to track and analyze the plastics in complex environments. However, many *in vitro* and *in vivo* data have been generated using fluorescent, spherically shaped, and commercially available polystyrene (PS) nanoparticles to study their uptake, kinetics, and effects.[22–24] In the vast majority of such studies, spherical model PS particles, generally containing fluorescent molecules that allow microscopic tracing, were used because they can readily be synthesized at various sizes[25–27] and are widely available from commercial suppliers. However, as a result of their popularity for single use products, polyethylene (PE) and polypropylene (PP) particles are much more abundant in the environment than PS,[12,28–30] and are therefore more likely to come into contact with humans (*i.e.* as a result of eating contaminated marine organisms). Furthermore, spherical particles are often not a good representation of particles found in the environment.[11,24,30]

The absence of more extensive risk assessment studies is perhaps related to the fact that researchers' access to nanoparticles of relevant plastics, particularly those that include a label for specific analytical methods, has been limited. A few groups have studied plastic nanoparticles made of polymers other than PS, and reported the creation of PET or PVC particles through laser ablation[31,32] or PET, PE, and nylon particles *via* chemical re-precipitation or microemulsions.[33–35] Some additional work has been done involving the chemical synthesis of PP particles[36] and the generation of PE particles through mechanical means.[37] However, the techniques used to characterize the particles presented in these studies are widely varied, and all the methods reported have only been tested for a limited number of plastic types.

The aim of this study was therefore to explore a versatile pathway to create plastic nanoparticles that also contain fluorescent molecules to facilitate their detection by fluorescence techniques. We elected to use PS, PP, and PET, which are widely used in packaging applications and represent different property profiles, and explored a sequence of processes that include melt-mixing the polymer with a fluorescent dye and subsequently milling the pellets produced. We used an array of standard techniques to characterize the nanoparticles and, in order to demonstrate the usefulness of the approach, the biocompatibility and cellular interaction of the nanoparticles were investigated using two relevant cell types (*i.e.* intestinal cells and macrophages) mimicking the first line of defense in the intestine.

2. Materials and methods

2.1. Materials

All water used in this study was purified with an 18.2 MΩ cm arium 611DI MilliQ system (Sartorius Stedim Biotech, Germany) prior to use. All chemicals were purchased from Sigma Aldrich (USA) unless stated otherwise.

Poly(ethylene terephthalate) (PET) (Goodfellow Cambridge Ltd., England), isotactic polypropylene (PP) (Sigma Aldrich, USA), and polystyrene (PS) (Sigma Aldrich, USA) pellets were purchased and used as received. The synthesis of the thermostable cyano-oligo(*p*-phenylene vinylene) fluorophore 1,4-bis(α-cyano-4-methoxystyryl)-2,5-dimethoxybenzene (C1RG) (Fig. S1†) was reported earlier.[38]

2.2. Melt-mixing methods

To pre-mix the polymers and the 1,4-bis(α-cyano-4-methoxystyryl)-2,5-dimethoxybenzene (C1RG) dye, thin films of the virgin polymers were prepared by compression molding 2.5 g of each polymer between Kapton sheets in a hot press (Carver, USA) at 200 (PS), 170 (PP), or 255 (PET) °C with a pressure of 2 metric tons for 1 minute and then 5 metric tons for an additional minute. The films were removed from the press and cooled to ambient temperature between the Kapton sheets. C1RG was sprinkled onto the polymer films in concentrations of 0.01% w/w for polystyrene (PSC1RG) and polypropylene (PPC1RG), and 0.1% for PET (PETC1RG). The films were then folded onto themselves and compression-molded again using the above parameters, before the materials were (separately) fed into a Haake Mini Lab II twin screw extruder

(Thermo Fisher, USA). Each material was subjected to two 5-minute mixing cycles under recycling conditions (200 (PS), 170 (PP), or 255 (PET) °C) prior to final extrusion (Table S1†). The extruded strands were cut into pellets. This protocol was repeated for each plastic type without the addition of C1RG to produce materials that had experienced the same process but were free of C1RG, which were used for control experiments.

2.3. Milling methods

Virgin polymer pellets and C1RG-containing polymer pellets were separately milled under liquid-nitrogen cooling in a 6770 Freezer Mill (steel milling rod; steel chamber plugs; polycarbonate chamber; SPEX, USA) in 2 cycles of 3 minute milling at 12 counts per second (CPS) with a 2 minute cooling cycle between the millings and a 15 minute pre-cooling to reduce their dimensions to the micrometer level. The cryo-milled particles thus produced were passed through a stainless-steel sieve with a 0.3 mm mesh (VWR International, USA) to ensure that the material met the size requirements for subsequent ball milling.

The sieved, cryo-milled plastic microparticle samples were further milled in a NanoWitt-Lab mill (Fig. S1†) using micron-sized zirconium dioxide beads (FREWITT SA, Switzerland). Thus, particle suspensions containing 10% w/w sodium dodecyl sulfate (SDS) and 8 g of the plastic microparticles in MilliQ water were mixed and loaded into the NanoWitt-Lab 100 milling chamber in batch mode with a milling bead ratio of 60% v/v. Optimized process parameters have been selected with a 4.7 m s^{-1} agitator speed and 500 micron milling beads. The suspension temperature has been kept stable at approx. 15 °C during the 3 hour milling cycle.

2.4. Dialysis methods

The ball milled suspensions were filtered through a Chromafil filter with a pore size of 0.2 μm (Macherey-Nagel, Germany) and placed into dialysis membranes with a 14 kDa cutoff (Carl Roth GmbH + Co, Switzerland). The dialysis membranes were submerged in 2 L of MilliQ water, which was changed daily. Conductivity measurements were conducted daily, and the dialysis was considered complete once the conductivity remained constant, typically after 3–4 days.

2.5. Attenuated total reflection Fourier transform infrared spectroscopy (ATR-FTIR)

Powders of filtered, dialyzed plastic particle suspensions after the ball milling step were obtained by drop-casting onto aluminum foil and drying in a desiccator. Additional powders for analysis were drop-cast as described above, but the filtering step was omitted before dialysis was conducted. Attenuated total reflection Fourier transform infrared spectroscopy (ATR-FTIR) was utilized to identify the chemical fingerprint of all particles. A Perkin Elmer (USA) Spectrum 65 FTIR spectrometer with a Perkin Elmer universal attenuated total reflection (UATR) accessory and pressure arm was used to collect a combination of 10 spectra from 4000 cm^{-1} to 650 cm^{-1} for every sample other than the filtered, dialyzed nano PSC1RG and filtered, dialyzed nano PPC1RG samples, which were averaged over 150 scans to account for their low concentration. The resulting spectra were analyzed with the accompanying Perkin Elmer Spectrum 10 software.

2.6. Fluorimetry

Samples of C1RG labelled and unlabeled PET, PP, and PS microparticles were prepared by mixing 30 mg of particles with 3 mL of complete Roswell Park Memorial Institute media (cRPMI) without phenol red to minimize fluorescence interference (Gibco, Switzerland). Samples of particles in cRPMI were heated to 37 °C and left for 24 hours in an oven (Memmert, Germany). After 24 hours, a 1.5 mL subsample was collected and filtered with a Chromafil filter with a pore size of 0.2 μm to remove the microparticles. Fluorescence emission intensity was measured on a Fluorolog TCSPC spectrofluorometer (Horiba, UK) with the accompanying FluorEssence software (v3.8). Measurements were obtained by exciting the materials with a 435 nm wavelength and a 1 nm entry slit width, and collecting emission from 450 nm to 800 nm with a 0.5 nm exit slit width. This process was repeated for a sample of particles incubated for 7 days at 37 °C. As a positive control, 30 mg of C1RG labelled and unlabeled PET, PP, and PS microparticles were left at room temperature in dichloromethane (DCM; Sigma Aldrich, USA) for 7 days. Additional control samples were prepared at the same concentrations in phosphate-buffered saline (PBS) and kept at 37 °C for 7 days. Measurements for all the samples were taken using the same wavelengths.

2.7. Polarized and depolarized dynamic light scattering (DLS, DDLS)

DLS data were collected for the filtered, dialyzed plastic nanoparticle dispersions, both with and without stabilization with 1% SDS, at constant temperature (21 °C) on a commercial goniometer instrument (3D LS Spectrometer, LS Instruments AG, Switzerland). The plastic nanoparticles were also dispersed in complete cell culture medium and measured with DDLS (ESI† section S4.4).

2.8. Scanning electron microscopy (SEM)

Plastic microparticle powders were placed onto aluminum SEM holders and 10 μL of ethanol was dropped onto the sample to distribute the particles evenly. Serial dilutions of the filtered, dialyzed plastic nanoparticle suspension were prepared at volume ratios of 1 : 10, 1 : 100, and 1 : 1000, and 5 μL of each dilution was placed onto a surface coated (Edding, Germany) SEM sample holder. As a control, 5 μL of MilliQ water was used.

All samples were dried overnight in a desiccator, sputter coated with a 2.5 nm thick layer of gold using a 208 HR sputter coater (Cressington Scientific Instruments, England), and

imaged with a Mira3 LM FE scanning electron microscope (pixel size: 0.0017 × 0.0017 μm^2; Tescan, Czech Republic).

2.9. Quartz crystal microbalance (QCM)

An OpenQCM quartz crystal microbalance (Novaetech S.r.l., Italy) with a 10 MHz crystal and an electrode area of 0.283 cm^2 was utilized to determine the concentration of 20 μL aliquots of plastic nanoparticle suspensions. Measurements were carried out at 37 °C. The frequency of the crystal was recorded prior to deposition (f_0), during deposition, and until all of the liquid had evaporated. Measurements were considered complete once the frequency had reached a new, stable value (f_e) (ESI† section S4.7). Measurements were carried out in triplicate for all of the particle types.

2.10. Cell cultures

The human colon (colorectal adenocarcinoma) cell line Caco-2 was obtained from the American Type Culture Collection (USA) and cultured in complete medium consisting of Dulbecco's modified Eagle medium (DMEM) (Gibco, Switzerland) supplemented with 10% non-heat inactivated fetal bovine serum (Gibco, Switzerland), 1% MEM nonessential amino acids (Gibco, Switzerland), 1% L-glutamine (Gibco, Switzerland), and 1% penicillin/streptomycin (Gibco). The complete medium is referred to as cDMEM. The cells were kept at 37 °C and 5% CO_2, grown in 75 cm^2 flasks (Corning, USA) and were sub-cultured twice per week at a ratio of 1 : 4. Experimental cells were grown on 12-well Transwell™ inserts with a 3 μm mean pore size and a 0.9 cm^2 surface area (Corning Incorporated, USA) placed in a 12-well plate and were allowed 3 weeks to fully differentiate prior to use in exposures. The medium was changed twice per week.

The mouse monocyte/macrophage cells (J774A.1 cell line; American Type Culture Collection from Rockville, MD) were grown in RPMI 1640 with HEPES (Gibco, Switzerland) supplemented with 10% fetal bovine serum (FBS, heat inactivated, PAA Laboratories, Austria), 1% L-glutamine (Gibco, Switzerland), and 1% penicillin/streptomycin (Gibco, Switzerland). The complete medium is referred to as cRPMI. Prior to particle exposure, the cells were seeded into 4-well glass chambers (Thermo Fisher Scientific, USA) at a density of 44 400 cells per cm^2. The J774A.1 macrophages were grown for 24 hours prior to further use.

2.11. Exposures

Dialyzed, filtered, non-surfactant-stabilized plastic nanoparticle suspensions were sonicated for 15 minutes before they were mixed at a 1 : 4 ratio with cell culture medium, giving final concentrations of 10.21 μg mL^{-1} for PETC1RG particles, 2.14 μg mL^{-1} for PPC1RG particles, and 1.20 μg mL^{-1} for PSC1RG particles. As a result of the differences in the yield after the ball milling experiments, these concentrations were the highest that could be obtained for each particle type without the risk of osmotic shock upon the addition of the suspensions into the cell cultures.

Caco-2 cells were exposed to plastic nanoparticles under pseudo-air liquid interface (pseudo-ALI) conditions (100 μL of medium mixed with particles in the apical compartment and 600 μL cDMEM in the basal) for 12–24 hours. J774A.1 macrophages were collected 24 hours after exposure. Additional wells for negative controls with only cell culture media and positive controls containing 0.2% TritonX in complete media were incubated for both cell types.

As an additional control, free C1RG dye (*i.e.* the crystalline powder) was mixed at a concentration of 0.1% by weight with water (*i.e.* 2.7 mg of C1RG in 2497 μL of MilliQ water) and the suspension was then sonicated 15 minutes prior to mixing 1 : 4 with cRPMI. J774A.1 cells were then exposed to 600 μL of the aqueous suspension containing free C1RG for 24 hours.

2.12. Confocal laser scanning microscopy (cLSM)

The cells were fixed using 4% paraformaldehyde (PFA) in PBS for 15 minutes prior to staining. The fixed cell samples were permeabilized with 0.2% TritonX in PBS for 15 minutes and stained with rhodamine phalloidin and DAPI for one hour. Prior to fixation and between each step, the cells were washed 3 times with PBS. The stained cell inserts were affixed to glass slides.

The stained cell samples were imaged with a Zeiss LSM 710 META confocal microscope (Carl-Zeiss AG, Germany). Excitation laser wavelengths of 488 nm (C1RG), 405 nm (DAPI) and 561 nm (rhodamine/phalloidin) were used.

2.13. Lactate dehydrogenase (LDH) assay

Basal media from Caco-2 cell cultures and media from J774A.1 were pipetted in 100 μL aliquots into a 96-well plate. Solutions from a Sigma Aldrich cytotoxicity detection kit (LDH, manufactured by Roche, Switzerland) were mixed according to the manufacturer's instructions. The media were combined with 100 μL of the LDH assay working solution. Endpoint measurements were taken with a Bio-Rad Benchmark Plus microplate spectrophotometer and the accompanying Bio-Rad Microplate Manager software. The absorbance was read at 490 nm (subtracting a 630 nm reference filter) in 30 second intervals. Measurements were conducted in triplicate.

2.14. Data processing

Fiji (ImageJ, version 1.52; NIH, USA) was used to measure the size of plastic particles present in SEM images. 1000 representative particles of each plastic nanoparticle type were measured to determine the final reported average diameters. Imaris (Bitplane, Switzerland) was used to process images obtained from cLSM and create 3D renderings. DLS and DDLS primary experimental and derived secondary data were regressed by using unconstrained linear and non-linear models weighted according to normally distributed variables using Mathematica (Wolfram Research Inc., version 11.3).

3. Results and discussion

3.1. Preparation and characterization of plastic particles

Virgin pellets of poly(ethylene terephthalate) (PET), polypropylene (PP), and polystyrene (PS) were successfully melt-mixed with 1,4-bis(α-cyano-4-methoxystyryl)-2,5-dimethoxybenzene (C1RG), a fluorescent dye that was selected due to its thermal stability and optical properties. All fluorescently labeled and virgin plastic pellets were milled under cryogenic conditions to obtain microparticles that had a maximum dimension of below 170 μm and were, if C1RG was incorporated, fluorescent. These properties were confirmed by SEM and cLSM imaging (ESI† section S2). Microparticles which were unlabeled and labelled with C1RG were then subjected to a leaching study prior to further processing. The fluorimetry data obtained showed that, even after 1 week of incubation at 37 °C, no free dye molecules could be detected in the PBS upon removal of the particles (Fig. 1). The maximum observed fluorescence emission in the positive control is at 503 nm, a value in good agreement with previously published data.[38] The overall intensity of the PETC1RG fluorescence emission in the positive control is higher as a result of the larger mass of dye that was melt processed into the material. Some autofluorescence of the cell culture media could still be seen in the 450 nm–570 nm range, likely the result of the presence of key nutrients such as riboflavin and folic acid which are known to be autofluorescent.[39,40] This slight autofluorescence is the only signal detected for all the cRPMI samples and indicates that no free dye molecules leak into the supernatant even under physiological conditions for 7 days.

Additionally, the surface chemistry of the resulting microparticles was probed with contact angle measurements, a technique which can be used to monitor changes in the wettability of a surface as a result of chemical alterations to the material it is composed of.[39] Melt-pressed films of unlabeled and C1RG labelled microparticles showed no statistically significant difference in their contact angles (*e.g.* unlabeled PP = 94° ± 4°, PPC1RG = 91° ± 4°, unlabeled PS = 83° ± 6°, PSC1RG

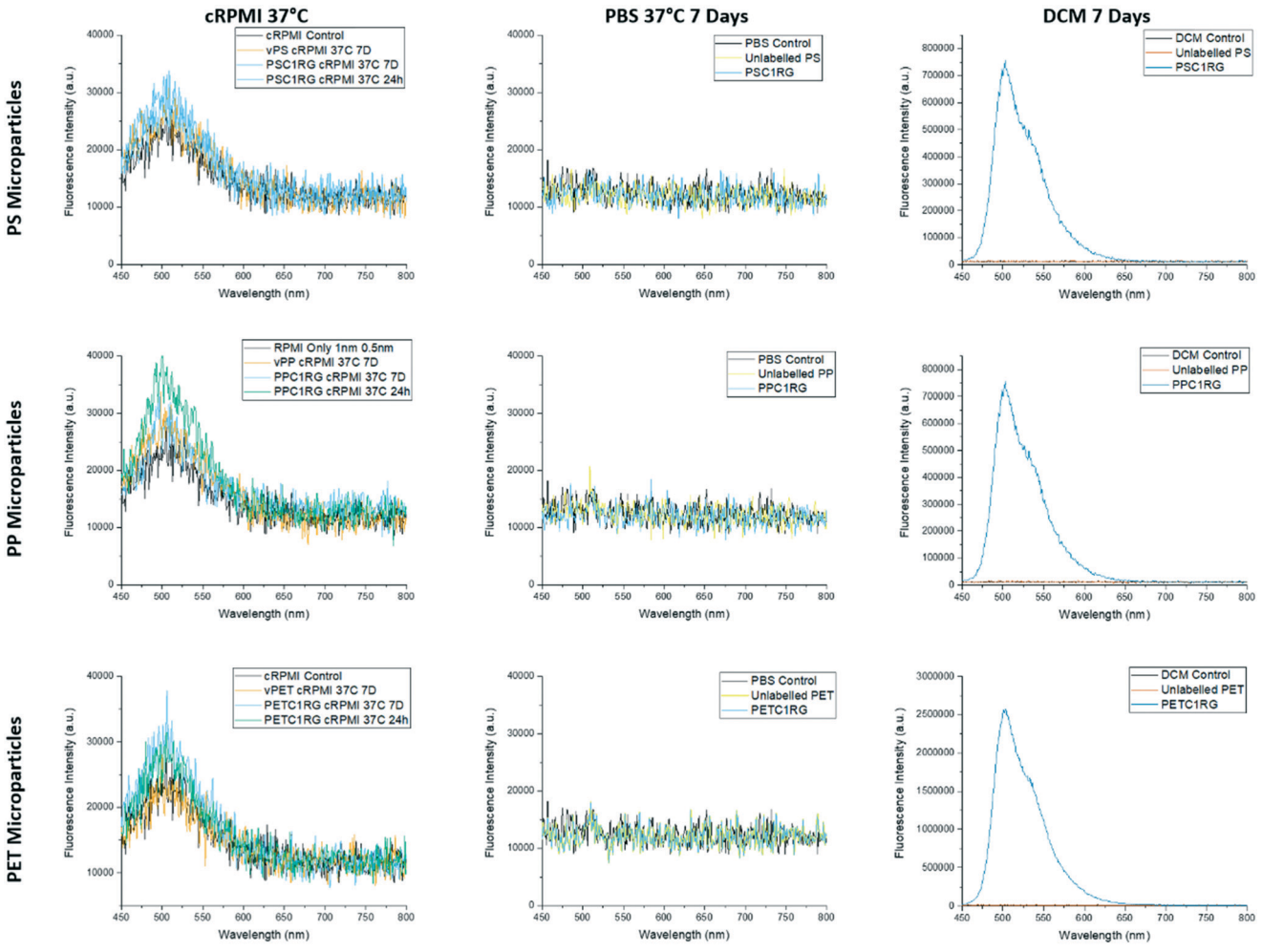

Fig. 1 Fluorophore leaching study using fluorimetry. Fluorescence intensity data of supernatants of C1RG labelled and unlabeled microplastic particles (PS, PP and PET) incubated for 24 h and 7 days at 37 °C in cRPMI were measured. The DCM exposed to C1RG labelled particles showed a significant difference in fluorescence intensity compared to the unlabeled particle samples in DCM and the negative control. Additional controls run in PBS at 37 °C for 7 days are shown in the central column, and no difference in fluorescence intensity was detected for any particle type.

= 86° ± 8°, unlabeled PET = 83° ± 5°, and PETC1RG = 81° ± 3° (ESI† section 2.4.)), indicating that the incorporation of C1RG into the polymers does not impact the surface properties of the particles produced. In the literature, chemical alteration of the surface of a polymer film through the use of plasma was shown to decrease the contact angle by as much as 48°.[41]

The microparticles of unlabeled PET, PET labeled with 0.1% C1RG (PETC1RG), PP labeled with 0.01% C1RG (PPC1RG), and PS labeled with 0.01% C1RG (PSC1RG) were then ball milled, filtered, and dialyzed to obtain plastic nanoparticles. As the unlabeled particles were only used as a negative control for initial imaging, only one plastic type, unlabeled PET, was milled. To ensure that the suspensions obtained after both milling steps contained only plastics, ATR-FTIR spectroscopy was used to obtain their chemical fingerprint. Additional analyses were carried out to confirm the presence of the nanoparticles and determine the average particle sizes, including SEM, cLSM, and light scattering.

From the initial polymer pellets to the final ball milled, filtered, and dialyzed plastic particle suspensions, the key ATR-FTIR peak locations remained the same for all the material types (Fig. 2 and ESI† section S3) and the spectra were void of the key peaks at 3495 cm^{-1} and 1553 cm^{-1} reported for the chemical fingerprints of zirconium oxide nanoparticles in the literature.[42] This result helped confirm the presence of plastic particles at all stages of the material processing protocol. However, some 'extra' peaks can be seen in the ball milled particle fingerprints (Fig. 2). Correlation values obtained from the Perkin Elmer Spectra 10 software indicate similarities with SDS of 7% for unlabelled PET, 16% for PETC1RG, 25% for PSC1RG, and 34% for PPC1RG, thus indicating that residual amounts of SDS may be adsorbed onto the particle surface. Peaks such as the one present in the PPC1RG spectra at 1735 cm^{-1} have been reported in the literature to be an indication of degradation of the polymeric backbone.[43] A similar indication of degradation can be seen in the altered crystallinity observed in the DSC data for PET particles (section S2.2†). Environmentally weathered plastics are also known to show altered crystallinity as a result of polymer degradation,[44,45] thus fitting the hypothesis that the presented material processing protocol would yield environmentally relevant model particles. Additionally, it is possible to adjust the melt processing protocols with additional pre-drying steps or lower mixing times to limit the amount of polymer degradation observed within the plastic micro- and nanoparticles obtained, or to alter their final crystallinity in order to study the impact of this material property on the plastic particle behavior, uptake, and/or cytotoxicity (section S2.2†).

For the visualization of the nanoplastic particles, confocal laser scanning microscopy was used. The cLSM images reveal the incorporation of the C1RG fluorophore into the plastic nanoparticles produced. These images also showed the presence of large aggregates (Fig. 3). It is important to note that a higher amount of C1RG was incorporated into PET particles (0.1%) which may make them appear brighter (Fig. 1).

Additional images obtained with SEM revealed a high heterogeneity in the plastic nanoparticles' shapes and sizes (Fig. 3), similar to that seen for environmentally collected plastic micro- and nanoparticles.[11,30] This heterogeneity is represented in the high standard deviation of the particles' maximum diameter measurements obtained using the SEM images: 71 ± 40 nm for PPC1RG, 70 ± 39 nm for PSC1RG, 62 ± 38 for unlabeled PET, and 74 ± 42 for PETC1RG nanoparticles (Table 1 and Fig. S6†).

DLS was used to measure the hydrodynamic radii of the particles and to determine their colloidal stability. Given that the sample particles exhibit arbitrary but convex shapes that are not elongated (*i.e.* not rods; Fig. 3), the characteristic dimensions of these plastic samples can be determined by relying on the concept of the hydrodynamic radius, which is a diffusion-equivalent metric. This approach is frequently used and represents an inherent characteristic of dynamic light scattering. It is evident that the data treatment of the plastic particles *via* the diffusion-equivalent sphere model is not accurate in the metrological sense, that is, the model is biased. Nonetheless, as with virtually any of the work reported on dynamic light scattering, such as addressing environmental samples[11] or gold nano-stars,[46] whether or not the dimensions of the particles dispersed in a given medium are on the nanoscale, and whether or not they are aggregated can safely be determined (Fig. S7†). The initial measurements of 1382 nm for PPC1RG and 4064 nm for PSC1RG indicated that they were colloidally unstable, likely as a result of their hydrophobicity (ESI† section S2.5), and required stabilization with the surfactant SDS. The final DLS measurements of surfactant stabilized particle dispersions (ESI† section S4.3) still give higher average particle diameters than those obtained from the SEM images: 220 nm for PPC1RG, 136 nm for PSC1RG, 146 nm for unlabeled PET, and 178 nm for PETC1RG (Table 1 and Fig. S7†). This is the result of the inherent differences between the measurement techniques, with light scattering providing a hydrodynamic size whose Rayleigh scattering value has a high dependence on the particle radius.[47]

The hydrodynamic radii were re-measured using DDLS. In the case of the semi-crystalline materials (*i.e.* PPC1RG, unlabeled PET, and PETC1RG (ESI† section S2)), the crystalline regions provided enough anisotropy for the scattering of the nanoparticles to be detected,[48] and diameters of 116 nm for PETC1RG, 120 nm for unlabeled PET, and 196 nm for stabilized PPC1RG particles were obtained. As PSC1RG particles were completely amorphous, they could not be sized (Fig. S7†).

Additionally, the colloidal stability of the nanoparticles in complete cell culture media was assessed *via* DLS measurements. PPC1RG and PSC1RG aggregated 5 minutes after being mixed with cDMEM, with the final measured sizes of the aggregates in the dispersions being 5958 nm and 5768 nm, respectively. The unlabeled PET particles showed a somewhat better colloidal stability; in this case, the diameter measured increased from 128 nm in water to 661 nm in cDMEM. The

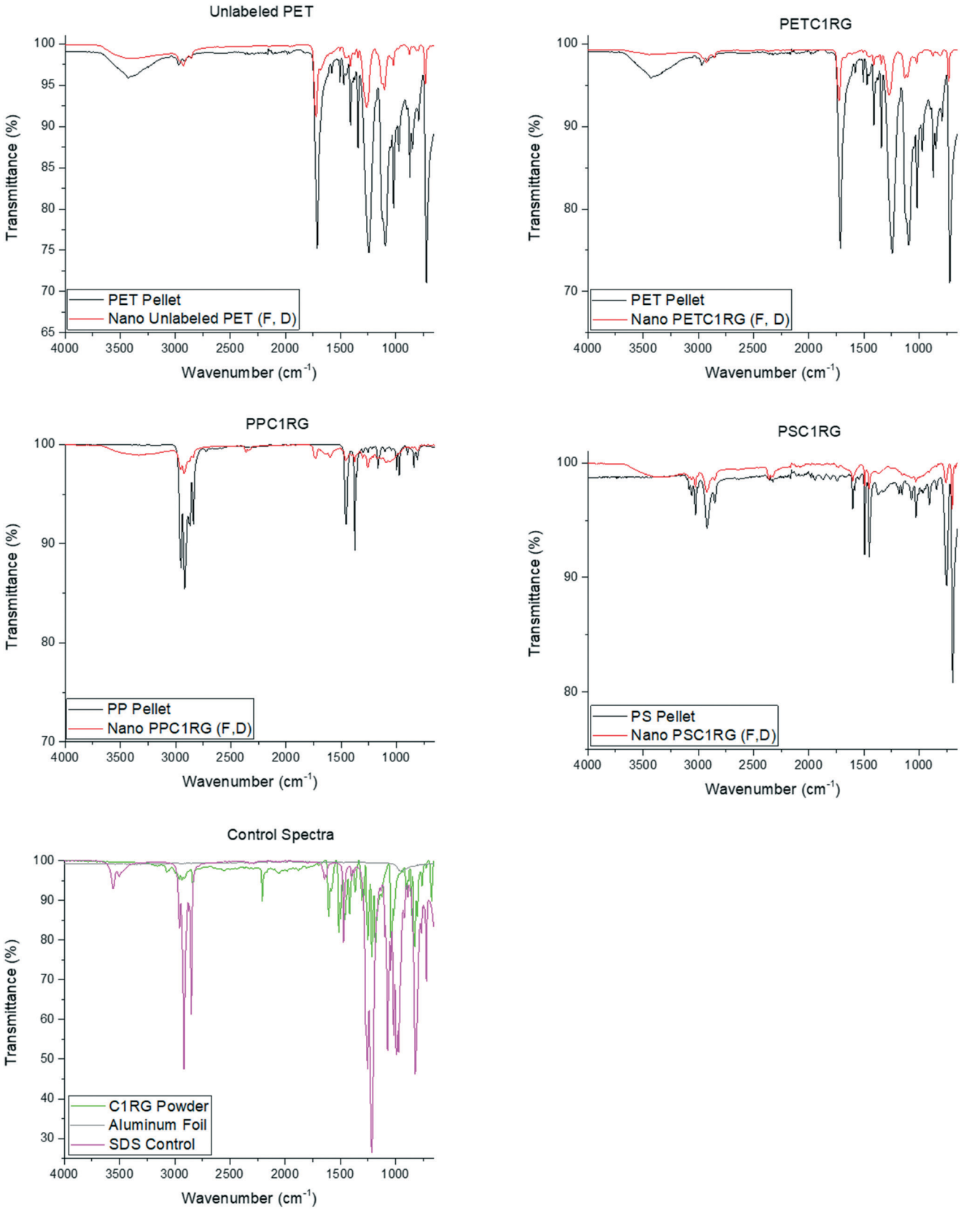

Fig. 2 Chemical fingerprints obtained with ATR-FTIR for each plastic particle type and the controls. The samples filtered and dialyzed prior to the measurement are denoted with (F, D) in the figure legends.

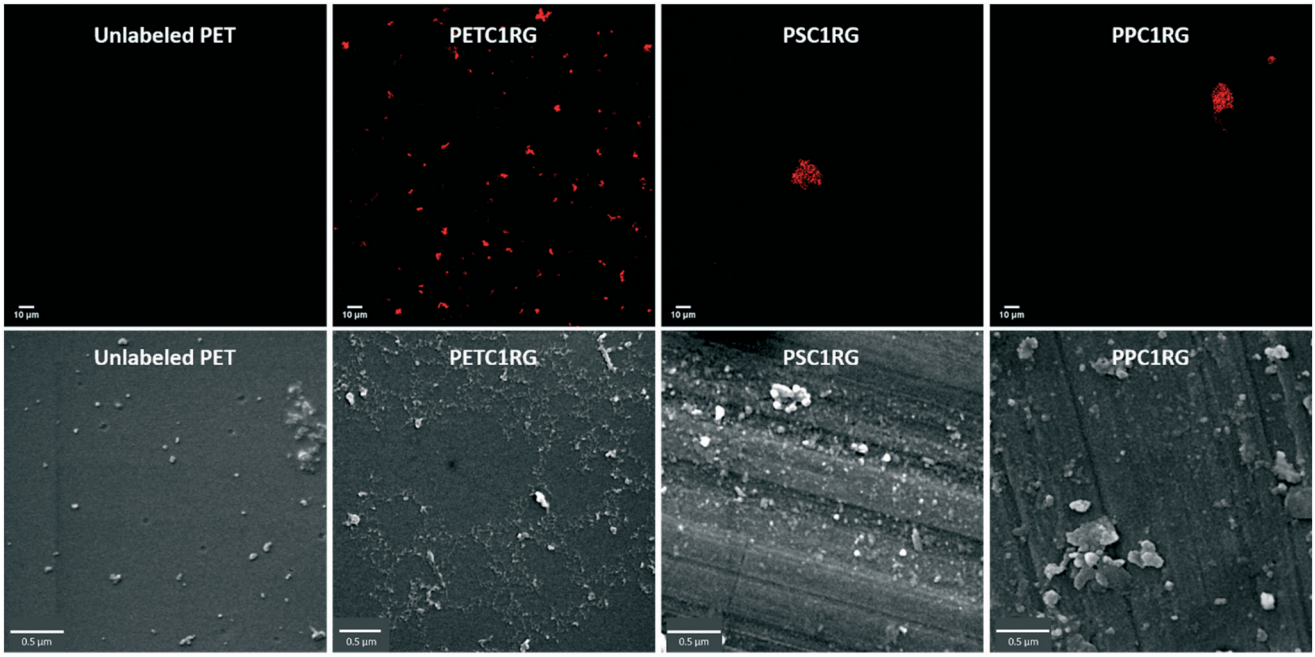

Fig. 3 Images of the nanoparticle dispersions obtained with a confocal laser scanning microscope using an excitation wavelength of 488 nm, shown in red (top row). Scale bar for all cLSM images: 10 μm. Bottom row: Scanning electron microscopy images for all plastic nanoparticles (1 : 10 dilution v/v with MilliQ water). Scale bar for all SEM images: 0.5 μm.

Table 1 A summary of all size and concentration measurement results for every plastic nanoparticle dispersion utilized in the study. Zeta potential (ζ-potential) measurements (section S4.3†) are also shown

Polymer	Concentration (μg mL^{-1})	SEM (nm)	DLS (nm)	DDLS (nm)	DLS in cDMEM (nm)	ζ-Potential (mV)
PPC1RG	8.6 ± 4.2	71 ± 40	1382 ± 166 220 ± 3[a]	196 ± 3[a]	5958 ± 923	−36[a]
PSC1RG	4.8 ± 1.2	70 ± 39	4064 ± 110 136 ± 1[a]	—	5768 ± 286	−43[a]
Unlabeled PET	31.7 ± 19.9	62 ± 38	146 ± 1	120 ± 4	661 ± 146	−29
PETC1RG	40.8 ± 19.3	74 ± 42	178 ± 1	116 ± 5	185 ± 4	−26

[a] Particle stabilization with 1% SDS was required to obtain accurate measurements.

PETC1RG particles showed the highest stability, with the initial measured diameter of 145 nm increasing slightly to 185 nm after their dispersion in cDMEM (ESI† section S4.6). This slight increase in particle size is likely the result of the formation of a protein corona around the particles[49] and also accounts for particles forming aggregate clusters. The higher stability of the PET particles in both water and cell culture media is likely the result of their lower hydrophobicity (Table S4 and Fig. S4†), particularly when compared to PP, which is in agreement with simulated values reported by Min *et al.*[50]

To obtain more quantitative information about the concentration of the nanoparticle dispersions, a QCM was used. The measurements showed that the dispersions were relatively dilute, with the highest concentration value obtained being 40.8 μg mL^{-1} for the PETC1RG nanoparticles (Table 1 and Fig. S9†). As the concentrations reported for each nanoplastic dispersion are, however, higher than those estimated for plastic nanoparticles within the environment (*i.e.* 1 ng mL^{-1}–1 μg mL^{-1} (ref. 51)) they were deemed viable for further work.

3.2. Plastic nanoparticle interactions with cells

To determine the biocompatibility of the PETC1RG, PPC1RG, and PSC1RG nanoparticles, two representative cell lines were selected for exposure studies. As one pathway for human exposure to plastic nanoparticles is *via* ingestion of contaminated foods or beverages, the biological barrier most likely to interact with plastic nanoparticles is the epithelial cell layer of the gastrointestinal (GI) tract. Particles which translocate the epithelial barrier would also have the potential to interact with immune cells such as macrophages. Thus, experiments were conducted using intestinal epithelial cells (*i.e.* Caco-2) as well as macrophages (*i.e.* J774A.1).

After incubation all particles (*i.e.* bare particles in cell culture media without surfactant stabilization) were observed both on the apical surface of the Caco-2 epithelial tissue (Fig. 4, yellow arrows) and inside the cells (Fig. 4, green arrows). For all the particle types, only a few aggregates could be located. In comparison, the J774A.1 cells after exposure to plastic nanoparticles showed numerous PETC1RG particles inside the cells (Fig. 4, green arrows). PSC1RG and PPC1RG particle aggregates were also found inside the cells, but less signal was detected in comparison to PETC1RG. The potential for this finding to be the result of the different concentrations of

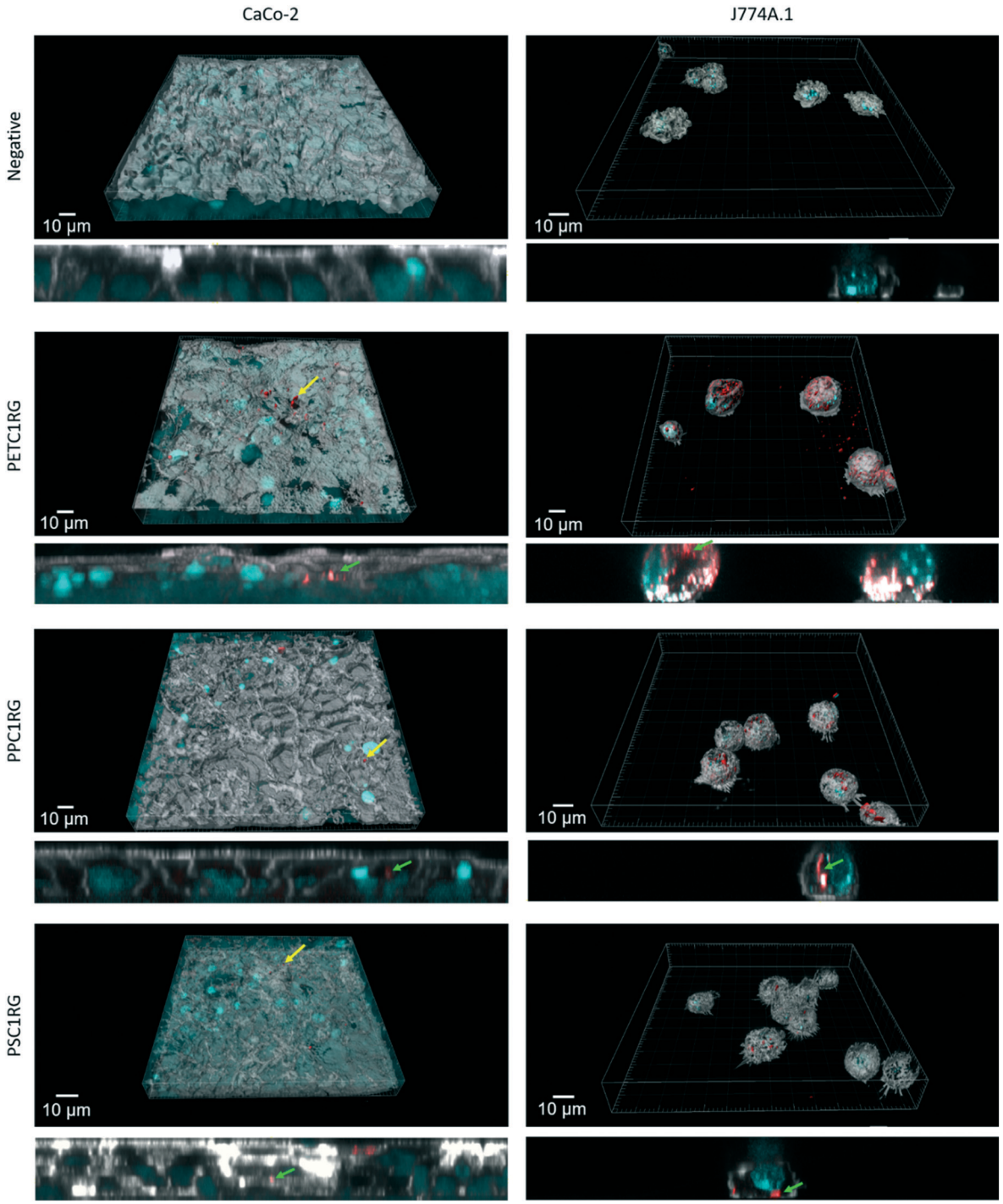

Fig. 4 Confocal laser scanning microscopy images of the Caco-2 (left column) and J774A.1 (right column) cells after exposure to the plastic nanoparticles. White: rhodamine/phalloidin. Blue: cyan. Red: C1RG. Yellow arrows are used to indicate representative areas of C1RG labelled plastic nanoparticle fluorescence outside the cells, while green arrows are used to indicate particles inside the cells. Images represent *xy* and *xz*-projections. Scale bars: 10 μm.

C1RG incorporated needs further investigation. Despite the differences in the plastic nanoparticle uptake, the cell culture media collected from the cell cultures, which were tested using the LDH assay, showed no induction of cytotoxicity for any particle or cell type when compared with the negative control (Fig. S10†). An additional exposure conducted with free C1RG powder showed that there was little to no dye uptake during a 24 hour period by the J774A.1 macrophages (Fig. S11†), thus indicating that false positive results caused by fluorophore leaching are unlikely.

4. Conclusions

The data presented herein showed that fluorescently labelled nanosized plastic particles could be derived using a combination of melt processing, cryo-milling, and ball milling. This protocol was shown to be highly versatile, with the nanoparticles created being composed of polymers ranging from PET to PP to PS. Additionally, it is possible to alter the particle brightness and color through the utilization of different amounts or types of thermostable fluorophores. However, further optimization of the milling procedure will likely be necessary to minimize the potential impact of surfactant contamination within the dialyzed nanoparticle dispersions (*e.g.* the use of a more biocompatible surfactant during ball milling, or more intensive cleaning protocols).

Despite this room for optimization, particle characterization results highlight the potential of the material processing protocol to create representative plastic nanoparticles that can be tracked in analytically complex environments such as cell cultures. Particle sizing by various methods revealed average sizes between 75 (SEM) and 222 (DLS) nm, with high variation between techniques that measured core sizes and those which measured hydrodynamic sizes. Leaching experiments confirmed that the dye molecules remained within the plastic particles even after their exposure to cRPMI at 37 °C for 7 days. Exposure to two representative cell types showed that none of the particles were cytotoxic, according to LDH data, for the herein used concentrations. Different interactions of the particles with the two cell types were observed; particles were found both on the apical surface and intracellularly in the intestinal tissue while many particles were found intracellularly in the macrophages.

Author contributions

R. L. made the study concept and supervised the experiments. J. C. was responsible for the creation of the plastic particles used in the study. Additionally, the SEM and cLSM images, leaching and light scattering data collection, and cell culture data were provided by J. C. The light scattering data were analyzed utilizing scripts and support provided by S. B. Support for suspension stabilization and ball milling was provided by C. R. and X. G. cLSM image analysis for the cell culture exposure data and their 3D reconstruction was done by D. S. The thermostable fluorophore C1RG and support for the material processing techniques were provided by C. W. B. R.-R. and A. P.-F. were the project's principal investigators. All authors contributed to the writing of the manuscript, and gave their approval to the final draft prior to publication.

Conflicts of interest

Christian Rhême and Xin Gao are employees of Frewitt SA. The other authors declare no competing financial interest.

Acknowledgements

The authors would like to thank the Adolphe Merkle Foundation for providing research funding and Frewitt SA for allowing the use of their milling equipment in their technical center and for their process support. Additionally, the authors thank Miguel Spuch-Calvar for assistance with the graphic design, and Veronique Buclin and Anita Roulin for assistance with the initial material processing. R. L. and D. S. acknowledge funding from SPARK by the Swiss National Science Foundation (190287 and 190440). Additionally, A. P.-F. acknowledges funding from the Swiss National Science Foundation (200020_184635).

References

1 PlasticsEurope, Plastics – the Facts 2019: An analysis of European plastics production, demand and waste data, in *Plastics – the Facts*, Brussels–Belgium, 2019, p. 39.
2 PlasticsEurope, Plastics – the Facts 2018: An analysis of European plastics production, demand and waste data, in *Plastics – the Facts*, Brussels–Belgium, 2018, p. 60.
3 R. Geyer, J. R. Jambeck and K. L. Law, Production, use, and fate of all plastics ever made, *Sci. Adv.*, 2017, **3**(7), e1700782.
4 J. R. Jambeck, *et al.*, Plastic waste inputs from land into the ocean, *Science*, 2015, **347**(6223), 768–771.
5 A. A. Horton, *et al.*, Microplastics in freshwater and terrestrial environments: Evaluating the current understanding to identify the knowledge gaps and future research priorities, *Sci. Total Environ.*, 2017, **586**, 127–141.
6 J. P. da Costa, *et al.*, (Nano)plastics in the environment – Sources, fates and effects, *Sci. Total Environ.*, 2016, **566–567**, 15–26.
7 A. L. Lusher, *et al.*, Microplastics in Arctic polar waters: the first reported values of particles in surface and sub-surface samples, *Sci. Rep.*, 2015, **5**(1), 14947.
8 R. Dris, *et al.*, Synthetic fibers in atmospheric fallout: A source of microplastics in the environment?, *Mar. Pollut. Bull.*, 2016, **104**(1), 290–293.
9 M. A. Browne, *et al.*, Accumulation of Microplastic on Shorelines Woldwide: Sources and Sinks, *Environ. Sci. Technol.*, 2011, **45**(21), 9175–9179.
10 S. Allen, *et al.*, Atmospheric transport and deposition of microplastics in a remote mountain catchment, *Nat. Geosci.*, 2019, **12**(5), 339–344.
11 A. Ter Halle, *et al.*, Nanoplastic in the North Atlantic Subtropical Gyre, *Environ. Sci. Technol.*, 2017, **51**(23), 13689–13697.

12 O. Güven, *et al.*, Microplastic litter composition of the Turkish territorial waters of the Mediterranean Sea, and its occurrence in the gastrointestinal tract of fish, *Environ. Pollut.*, 2017, **223**, 286–294.
13 E. R. Holland, M. L. Mallory and D. Shutler, Plastics and other anthropogenic debris in freshwater birds from Canada, *Sci. Total Environ.*, 2016, **571**, 251–258.
14 L. Van Cauwenberghe, *et al.*, Microplastics are taken up by mussels(Mytilus edulis) and lugworms(Arenicola marina) living in natural habitats, *Environ. Pollut.*, 2015, **199**, 10–17.
15 N. von Moos, P. Burkhardt-Holm and A. Köhler, Uptake and Effects of Microplastics on Cells and Tissue of the Blue Mussel Mytilus edulis L. after an Experimental Exposure, *Environ. Sci. Technol.*, 2012, **46**(20), 11327–11335.
16 A. J. R. Watts, *et al.*, Ingestion of Plastic Microfibers by the Crab Carcinus maenas and Its Effect on Food Consumption and Energy Balance, *Environ. Sci. Technol.*, 2015, **49**(24), 14597–14604.
17 E. Besseling, *et al.*, Nanoplastic Affects Growth of S. obliquus and Reproduction of D. magna, *Environ. Sci. Technol.*, 2014, **48**(20), 12336–12343.
18 J. Li, *et al.*, Microplastics in commercial bivalves from China, *Environ. Pollut.*, 2015, **207**, 190–195.
19 L. M. Hernandez, *et al.*, Plastic Teabags Release Billions of Microparticles and Nanoparticles into Tea, *Environ. Sci. Technol.*, 2019, **53**(21), 12300–12310.
20 S. A. Mason, V. G. Welch and J. Neratko, Synthetic Polymer Contamination in Bottled Water, *Front. Chem.*, 2018, **6**, 407.
21 K. D. Cox, *et al.*, Human Consumption of Microplastics, *Environ. Sci. Technol.*, 2019, **53**(12), 7068–7074.
22 H. J. Johnston, *et al.*, Evaluating the uptake and intracellular fate of polystyrene nanoparticles by primary and hepatocyte cell lines in vitro, *Toxicol. Appl. Pharmacol.*, 2010, **242**(1), 66–78.
23 M. Ekkapongpisit, *et al.*, Biocompatibility, endocytosis, and intracellular trafficking of mesoporous silica and polystyrene nanoparticles in ovarian cancer cells: effects of size and surface charge groups, *Int. J. Nanomed.*, 2012, **7**, 4147–4158.
24 R. Lehner, *et al.*, Emergence of Nanoplastic in the Environment and Possible Impact on Human Health, *Environ. Sci. Technol.*, 2019, **53**(4), 1748–1765.
25 H. Fritz, M. Maier and E. Bayer, Cationic Polystyrene Nanoparticles: Preparation and Characterization of a Model Drug Carrier System for Antisense Oligonucleotides, *J. Colloid Interface Sci.*, 1997, **195**(2), 272–288.
26 J. Jiang and S. Thayumanavan, Synthesis and Characterization of Amine-Functionalized Polystyrene Nanoparticles, *Macromolecules*, 2005, **38**(14), 5886–5891.
27 S. B. Brijmohan, *et al.*, Synthesis and Characterization of Cross-linked Sulfonated Polystyrene Nanoparticles, *Ind. Eng. Chem. Res.*, 2005, **44**(21), 8039–8045.
28 L. Lebreton, *et al.*, Evidence that the Great Pacific Garbage Patch is rapidly accumulating plastic, *Sci. Rep.*, 2018, **8**(1), 4666.
29 M. Baini, *et al.*, Abundance and characterization of microplastics in the coastal waters of Tuscany(Italy): The application of the MSFD monitoring protocol in the Mediterranean Sea, *Mar. Pollut. Bull.*, 2018, **133**, 543–552.
30 J. Caldwell, *et al.*, Assessing meso- and microplastic pollution in the Ligurian and Tyrrhenian Seas, *Mar. Pollut. Bull.*, 2019, **149**, 110572.
31 D. Magrì, *et al.*, Laser Ablation as a Versatile Tool To Mimic Polyethylene Terephthalate Nanoplastic Pollutants: Characterization and Toxicology Assessment, *ACS Nano*, 2018, **12**(8), 7690–7700.
32 H. M. Jawad, I. H. Shallal and M. H. Hassoni, Experimental and theoretical study of(PVC) nanoparticles prepared by laser ablation in ethanol, *AIP Conf. Proc.*, 2019, **2123**(1), 020101.
33 A. G. Rodríguez-Hernández, *et al.*, A novel and simple method for polyethylene terephthalate(PET) nanoparticle production, *Environ. Sci.: Nano*, 2019, **6**(7), 2031–2036.
34 G. Balakrishnan, *et al.*, Towards more realistic reference microplastics and nanoplastics: preparation of polyethylene micro/nanoparticles with a biosurfactant, *Environ. Sci.: Nano*, 2019, **6**(1), 315–324.
35 D. Crespy and K. Landfester, Preparation of Nylon 6 Nanoparticles and Nanocapsules by Two Novel Miniemulsion/Solvent Displacement Hybrid Techniques, *Macromol. Chem. Phys.*, 2007, **208**(5), 457–466.
36 P. Paik and K. K. Kar, Polypropylene nanosphere: particle size and crystal structure, *Int. J. Plast. Technol.*, 2009, **13**(1), 68.
37 H. El Hadri, *et al.*, Nanoplastic from mechanically degraded primary and secondary microplastics for environmental assessments, *NanoImpact*, 2020, **17**, 100206.
38 M. Kinami, B. R. Crenshaw and C. Weder, Polyesters with Built-in Threshold Temperature and Deformation Sensors, *Chem. Mater.*, 2006, **18**(4), 946–955.
39 A. Tyagi and A. Penzkofer, Fluorescence spectroscopic behaviour of folic acid, *Chem. Phys.*, 2010, **367**(2), 83–92.
40 M. Sun, T. A. Moore and P.-S. Song, Molecular luminescence studies of flavines. I. Excited states of flavines, *J. Am. Chem. Soc.*, 1972, **94**(5), 1730–1740.
41 N. De Geyter, R. Morent and C. Leys, Surface characterization of plasma-modified polyethylene by contact angle experiments and ATR-FTIR spectroscopy, *Surf. Interface Anal.*, 2008, **40**(3–4), 608–611.
42 A. K. Singh and U. T. Nakate, Microwave Synthesis, Characterization, and Photoluminescence Properties of Nanocrystalline Zirconia, *Sci. World J.*, 2014, **2014**, 349457.
43 J.-L. Philippart, *et al.*, Influence of the exposure parameters on the mechanism of photooxidation of polypropylene, *Polym. Degrad. Stab.*, 1999, **64**(2), 213–225.
44 A. Ter Halle, *et al.*, To what extent are microplastics from the open ocean weathered?, *Environ. Pollut.*, 2017, **227**, 167–174.
45 C. J. Garvey, *et al.*, Molecular-Scale Understanding of the Embrittlement in Polyethylene Ocean Debris, *Environ. Sci. Technol.*, 2020, 11173–11181.
46 H. Jo, *et al.*, Ultra-effective photothermal therapy for prostate cancer cells using dual aptamer-modified gold nanostars, *J. Mater. Chem. B*, 2014, **2**(30), 4862–4867.

47 J. Stetefeld, S. A. McKenna and T. R. Patel, Dynamic light scattering: a practical guide and applications in biomedical sciences, *Biophys. Rev.*, 2016, **8**(4), 409–427.
48 S. Balog, *et al.*, Characterizing nanoparticles in complex biological media and physiological fluids with depolarized dynamic light scattering, *Nanoscale*, 2015, **7**(14), 5991–5997.
49 J. Fatisson, *et al.*, Physicochemical characterization of engineered nanoparticles under physiological conditions: Effect of culture media components and particle surface coating, *Colloids Surf., B*, 2012, **91**, 198–204.
50 K. Min, J. D. Cuiffi and R. T. Mathers, Ranking environmental degradation trends of plastic marine debris based on physical properties and molecular structure, *Nat. Commun.*, 2020, **11**(1), 727.
51 R. Lenz, K. Enders and T. G. Nielsen, Microplastic exposure studies should be environmentally realistic, *Proc. Natl. Acad. Sci. U. S. A.*, 2016, **113**(29), E4121–E4122.